JOURNAL OF RESEARCH of the National Bureau of Standards — C. Engineering and Instrumentation
Vol. 75C, No. 1, January-March 1971

Design and Operational Characteristics of a High-Speed (Millisecond) System for the Measurement of Thermophysical Properties at High Temperatures*

Ared Cezairliyan

Institute for Materials Research, National Bureau of Standards, Washington, D.C. 20234

(November 19, 1970)

Design and constructional details of a high-speed system for the measurement of selected thermophysical properties of electrical conductors at temperatures above 2000 K in experiments of subsecond duration are described. Operational characteristics of such a system are given. Various phenomena that affect the design and successful operation of the system are discussed and, whenever possible, quantitative results are given. Certain experimental checks to assess the operation of the system are also described.

Key words: High-speed measurements; high temperatures; thermodynamics; thermophysical properties.

1. Introduction

Interest in thermophysical properties at temperatures above the limit of accurate steady-state experiments has necessitated the development of high-speed measurement techniques. Most of the difficulties inherent in steady-state methods are eliminated in high-speed experiments. However, new problems arise due to the nature of rapid experiments, some of which increase rapidly with increasing speed. This suggests that an optimized system has to be designed for most accurate measurements.

The objective of this writing is to describe the details of a high-speed system for the measurement of selected thermophysical and related properties (heat capacity, electrical resistivity, hemispherical total and normal spectral emittances, melting point, etc.) of electrical conductors at temperatures above 2000 K in experiments of subsecond duration. Operational characteristics of such a system under actual experimental conditions are presented. Various phenomena that affect the design and successful operation of the system are discussed in the context of high-speed experiments and, whenever possible, quantitative results are given. Certain experimental checks to assess the operation of the system are described.

The method employed in the high-speed measurements is based upon rapid resistive heating of the specimen by a single pulse (subsecond duration) of direct current and measuring the pertinent quantities with millisecond resolution. Formulation of the relationships between various experimental quantities and properties is given in another publication [1][1]

* This work was supported in part by the Propulsion Division of the U. S. Air Force Office of Scientific Research under Contract ISSA-70-0002.

[1] Figures in brackets indicate the literature references at the end of this paper.

2. Measurement System

The high-speed measurement system consists of an electric power pulsing circuit and associated measuring and control circuits. A functional diagram of the complete system and a photograph of a portion of the system are presented in figures 1 and 2, respectively.

2.1. Pulsing Circuit

The pulse circuit includes the specimen in series with a battery bank, a standard resistance, a variable resistance, and a switching system. The battery bank consists of 14 series-connected 2 V batteries each having approximately 1100 A–h capacity. A standard resistance (0.001 Ω shunt) made of manganin strip is used to measure the pulse current flowing through the specimen. A variable resistance made of water-cooled Inconel tubes (total resistance = 30 mΩ) enables control of the heating rate of the specimen and the shape of the current pulse. The switching system consists of two series-connected, fast-acting switches. The second switch is used as a backup in the event the first one fails to open at the end of the heating period. The switches are operated by a series of pulse control units.

The pulsing circuit is a simple RL circuit whose dynamic characteristics, after closing of the switch, may be expressed by

$$E - L\frac{di}{dt} = i\,(R_s + R_c) \qquad (1)$$

where

R_s = resistance of the specimen
R_c = resistance of the circuit with the exception of the specimen

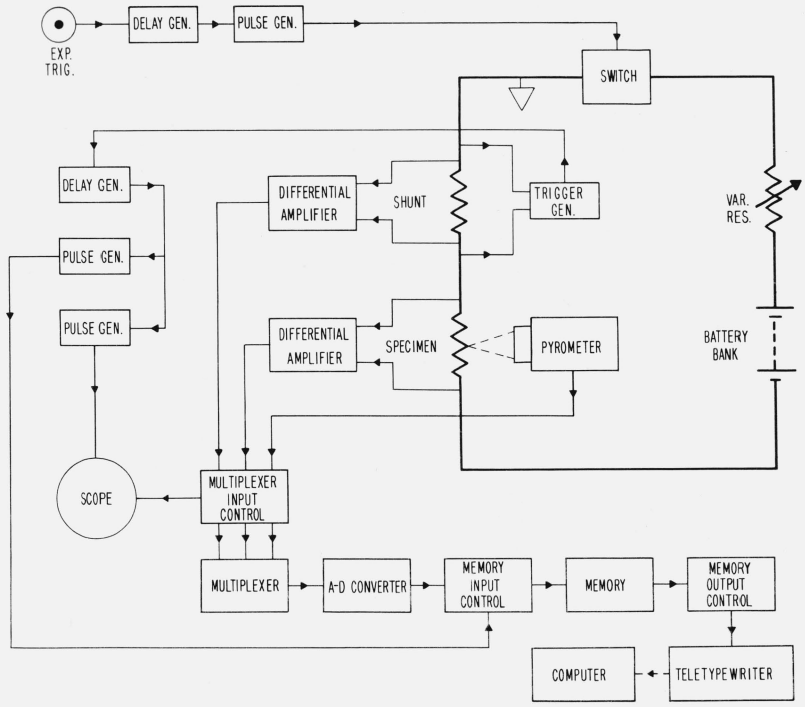

FIGURE 1. *Functional diagram of the complete high-speed measurement system.*

L = self-inductance of the complete circuit
E = battery potential
i = instantaneous current
t = time.

The solution of eq (1) is

$$i = \frac{E}{R}(1 - e^{-Rt/L}) \qquad (2)$$

where R = resistance of the complete circuit ($R = R_s + R_c$). Equation (2), which gives the increase of current as a function of time, is obtained on the assumption that the quantities E, L, and R are constant. In an actual experiment, this assumption is satisfied approximately for E and L, however, R increases with time as the specimen is heated. Therefore, the current versus time relationship is of a distorted exponential form. The circuit's "time constant," which is expressed by the quantity L/R, decreases with increasing R as the specimen is heated.

Energy stored in the magnetic field of an inductor, with no ferromagnetic material in its vicinity, is given by

$$W = \frac{Li^2}{2}. \qquad (3)$$

It may be noted that stored energy depends on the instantaneous value of the current and not on the current history. In a typical high-speed measurement system, in which inductance of the specimen is of the order of 10^{-7} H, and current is the order of 10^3 A, magnetic energy is of the order of 0.1 J. This is small compared to imparted energy, which is the order of 10^3 J. For a complete cycle of operation, consisting of closing the switch and after a finite period opening the switch, the stored energy in the specimen is zero.

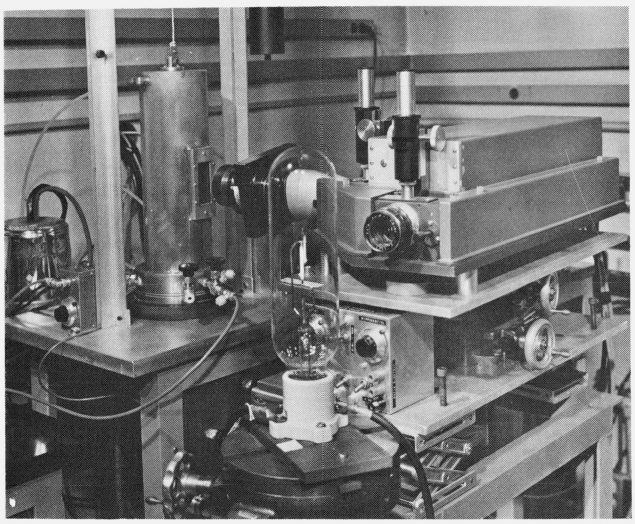

FIGURE 2. *The experiment chamber and the high-speed pyrometer.*

2.2. Measuring and Control Circuits

Voltage signals from both the standard resistance and the specimen are sent to the recording system via differential amplifiers. A potentiometric system is used to calibrate pulse-voltage and pulse-current measuring circuits including the differential amplifiers and the digital

recording system. A Kelvin bridge is used to measure resistance of the specimen at ambient temperature before and after a pulse experiment. A 400 Hz synchronous motor used in the high-speed pyrometer provides the time base for the data acquisition system. Timing of various events, such as closing of the switch and triggering of various electronic equipment, during a pulse experiment is achieved by a series of time-delay units. Triggering of the recording system and opening of the switch at the end of the desired heating period are automatically activated when the specimen temperature reaches preadjusted initial and final values.

2.3. Specimen

The specimen is a tube of the following nominal dimensions: length = 4 in (102 mm), outside diameter = 0.25 in (6.3 mm), wall thickness = 0.02 in (0.5 mm). A small rectangular hole (1 × 0.5 mm) is fabricated in the wall at the middle of the specimen to approximate blackbody conditions. In order to compensate for the cross-sectional nonuniformity created by the hole, a portion from the rest of the specimen is removed by grinding its surface. The criterion is that the cross section of the removed portion is equal to that of the opening created by the hole. From geometrical considerations this may be expressed as

$$ab = \frac{R^2}{2}\left(\frac{\pi\theta}{180} - \sin\theta\right) \tag{4}$$

where

a = width of hole
b = depth of hole (thickness of tubular specimen)
R = outer radius of specimen
θ = angle subtended by the arc corresponding to the ground flat.

After solving the above transcendental equation for the angle θ by iteration, the pertinent dimensions as shown in figure 3 may be obtained from the following relations:

$$L = 2R \sin\frac{\theta}{2} \tag{5}$$

$$C = R \cos\frac{\theta}{2}. \tag{6}$$

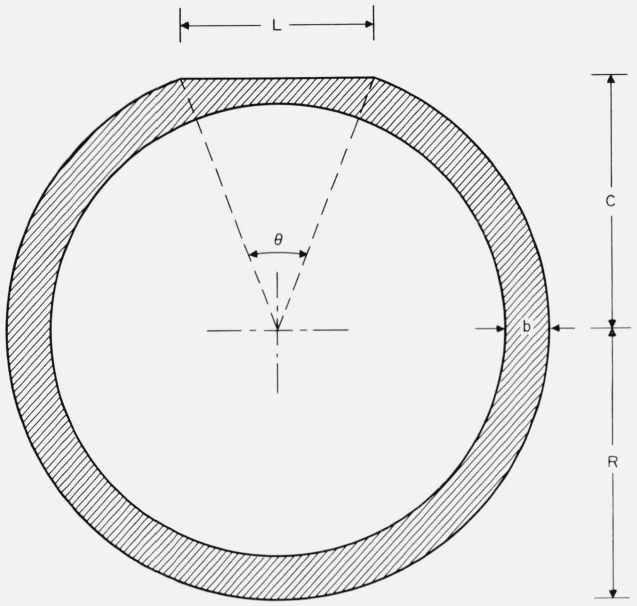

FIGURE 3. *Specimen cross section at the plane of the flat.*

A photograph of the specimen is shown in figure 4.

The rectangular sighting hole in the specimen wall is fabricated 0.8 mm offcenter to improve the blackbody quality. For the specimen geometry given in an earlier section, blackbody quality of the hole is estimated using De Vos' [10] method. Computations are made assuming four different specimen inner surface reflectances and for two specimen lengths, one corresponding to the "effective" length and the other to the actual length. The results (fig. 5) do not show any appreciable dependence of the blackbody quality on length and reflectance.

2.4. Experiment Chamber

The experiment chamber, shown schematically in figure 6, contains the specimen, the clamping electrodes, an expansion joint, potential probes, and other auxiliary components.

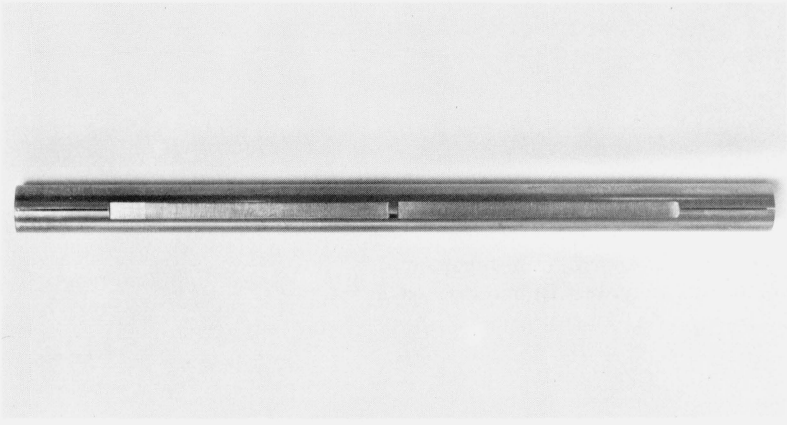

FIGURE 4. *Photograph of the specimen.*

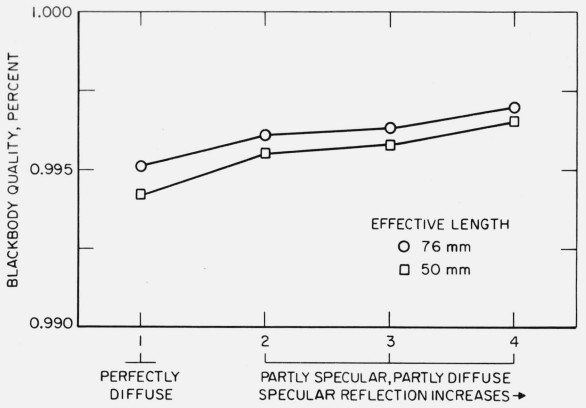

FIGURE 5. *Blackbody quality of a specimen computed for different inner wall reflectances and lengths.*

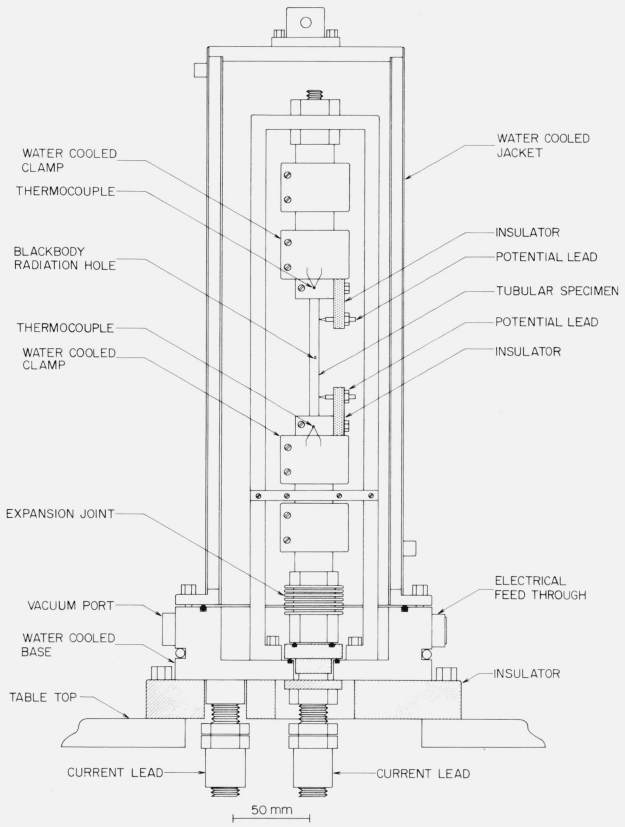

FIGURE 6. *Experiment chamber.*

The specimen is mounted vertically 6 mm offcenter with respect to the axis of the chamber to reduce the effect of internal reflections. The inner wall of the chamber is coated with nonreflecting paint. The chamber wall, as well as the specimen clamps, are water cooled. Thermocouples are connected (electrically insulated) to the two end clamps to measure the specimen temperature before each pulse experiment. An expansion joint allows the expansion of the specimen in the downward direction. The effect of specimen evaporation on the window transmission is minimized by placing a flat partial shield in front of the specimen.

The potential probes are knife-edges made of the specimen material and are placed at a distance approximately 13 mm from the end clamps. The knife-edges define an "effective" portion of the specimen, which should be free of axial temperature gradients for the duration of the experiment. A photograph of the specimen with the clamps and potential probes is shown in figure 7.

The chamber is designed for conducting experiments with the specimen either in vacuum or in a controlled atmosphere.

2.5. High-Speed Pyrometer

Temperature of the specimen is measured with a high-speed photoelectric pyrometer, which permits 1200 evaluations of the specimen temperature per second. The pyrometer alternately passes precisely timed samples of radiance from the specimen and a reference source through an interference filter (wavelength 650 nm, bandwidth 10 nm) to a photomultiplier. During each exposure the photomultiplier output is integrated and is recorded. Successive exposures to the reference source, which is a calibrated, gas-filled tungsten-filament lamp, are taken through a sequence of three different optical attenuators mounted on a rotating disk, resulting in a staircase of reference exposures with approximately 50 percent at-

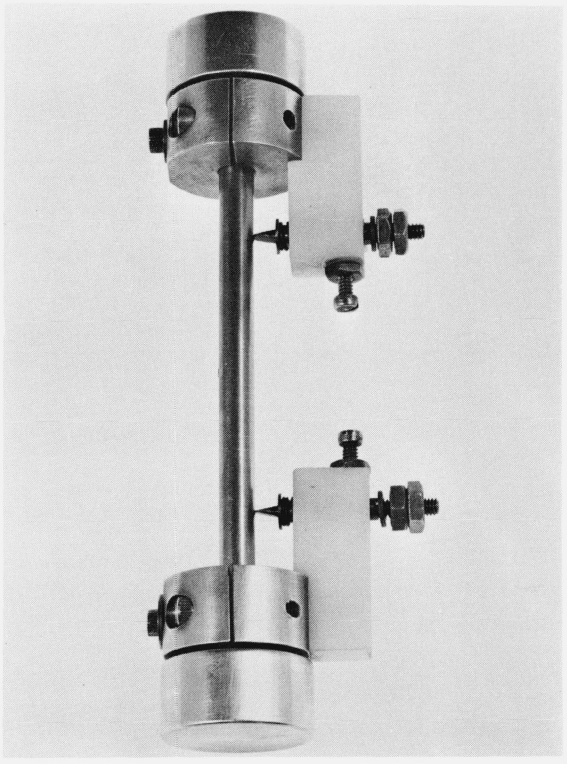

FIGURE 7. *Photograph of the specimen, clamps, and potential probes.*

tenuation for each step. This scheme is used for measurements up to 2500 K, the limit of reliable operation of gas-filled lamps. For measurements at higher temperatures calibrated optical attenuators are placed in the path of the radiation from the specimen. The details regarding the construction and operation of the pyrometer are given in the literature [2].

2.6. High-Speed Digital Data Acquisition System

The high-speed digital data acquisition system consists of a multiplexer, analog-to-digital converter, and a core memory together with control and interfacing equipment. All signals are brought to the multiplexer through differential amplifiers in order to avoid inaccuracies arising from common ground points. The multiplexed signals go to the analog-to-digital converter, which has a full scale reading of $\pm$ 10 V and a full-scale resolution of one part in 8192 ($8192 = 2^{13}$). Digital output from the converter consists of 13 binary bits plus a sign bit. This output is stored in a core memory having a capacity of 2048 words of sixteen bits each. The data acquisition system is capable of recording a set of signals corresponding to temperature, voltage, and current approximately every 0.4 ms. At the end of the pulse experiment, information stored in the memory is retrieved in the form of numeric printing and punched tape using a teletypewriter. Since the laboratory has access to a time-shared computer, it is possible to unload the memory directly to the computer, bypassing the intermediate stage of punching paper tape. A manuscript regarding the constructional and operational details of the high-speed digital data acquisition system is in preparation [3]. Oscilloscopes are used only to monitor the general pattern of the experimental results, and to detect any anomalies.

3. Operational Characteristics

Highest measurement precision is achieved when the experimental quantities are recorded close to the full-scale value of the data acquisition system. However, since quantities vary with time it is not possible to realize this completely. The recording of current can be optimized by adjusting the series resistance, which minimizes this variation. Also, the proper adjustment of the series resistance assures the quasi-linear variation of both voltage and current pulses. Oscilloscope trace photographs of typical voltage and current pulses are shown in figure 8. Radiance from the blackbody hole in the specimen, as well as that of the reference lamp, as seen by the pyrometer as a function of time is shown in figure 9. Dots forming the horizontal lines correspond to the three reference radiances. Temperature of the specimen is computed from the interpolation of its radiance between adjacent reference radiances.

In the computation of properties third-degree polynomial functions for voltage, current, and temperature as functions of time are obtained by least squares approximation of the data. Typical standard deviation of an individual point from the pertinent function is 0.02 percent for voltage, 0.03 percent for current, and 0.5 K for temperature.

Typical results on imparted power to the specimen, the heating rate of the specimen and the ratio of heating to cooling rate (M) for a molybdenum specimen computed from measurements of voltage, current, and temperature are shown in figures 10, 11, and 12, respectively. They represent a total of 40 experiments that were performed at two different speeds, designated as "fast" and "slow," over the temperature range 1900 to 2800 K. The smooth curves shown in the figures are obtained by fitting the computed points to third-degree polynomial functions using least squares approximation. The standard deviation of an individual point from the pertinent function is 0.5 percent for power, 0.7 percent for heating rate, and 0.8 percent for the ratio of heating to cooling rate. The small values of the standard deviations are an indication of the high degree of reproducibility of the current pulses and

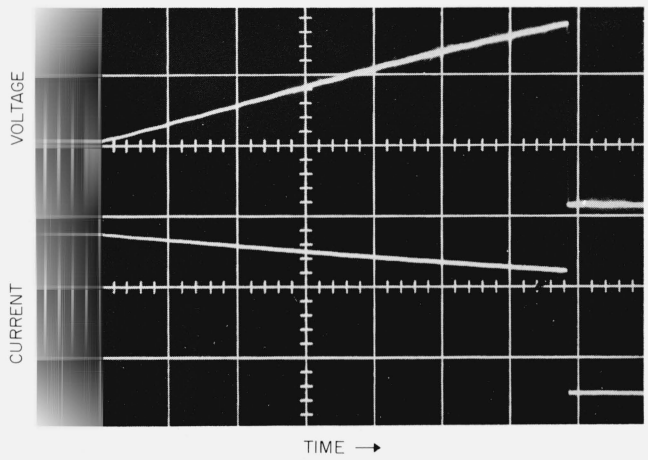

FIGURE 8. *Oscilloscope trace photographs of typical voltage and current pulses.*

Equivalence of each major division is: time = 50 ms, voltage = 2 V, current = 1000 A.

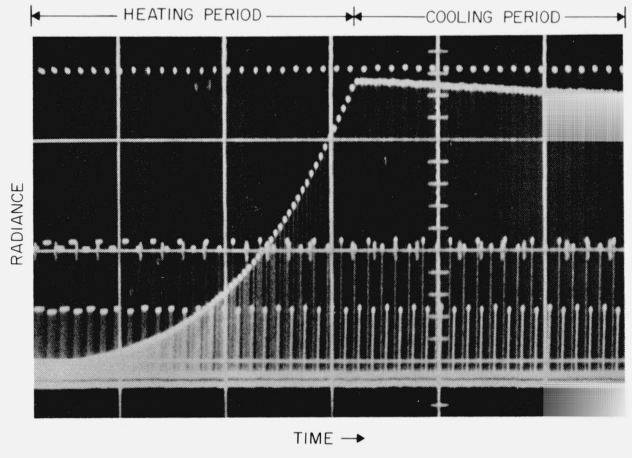

FIGURE 9. *Oscilloscope trace photograph of radiance of rapidly heating specimen.*

Dots forming the long horizontal lines correspond to radiances from the reference source. Equivalence of each major division is: time = 20 ms, radiance = arbitrary unit.

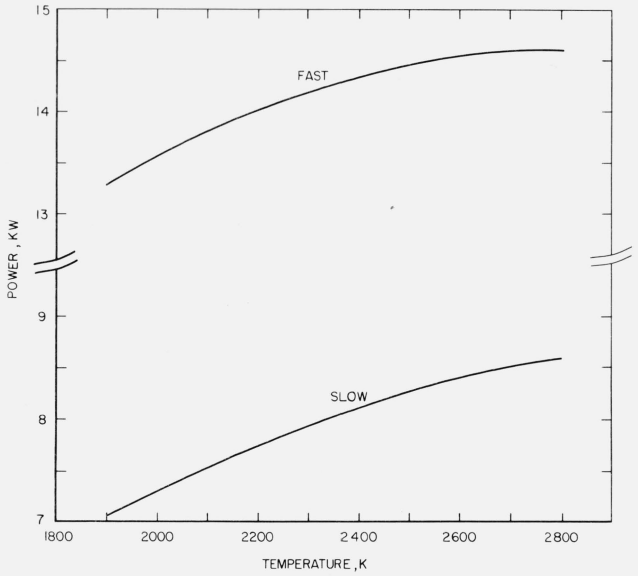

FIGURE 10. *Variation of the power imparted to a molybdenum specimen as a function of temperature.*

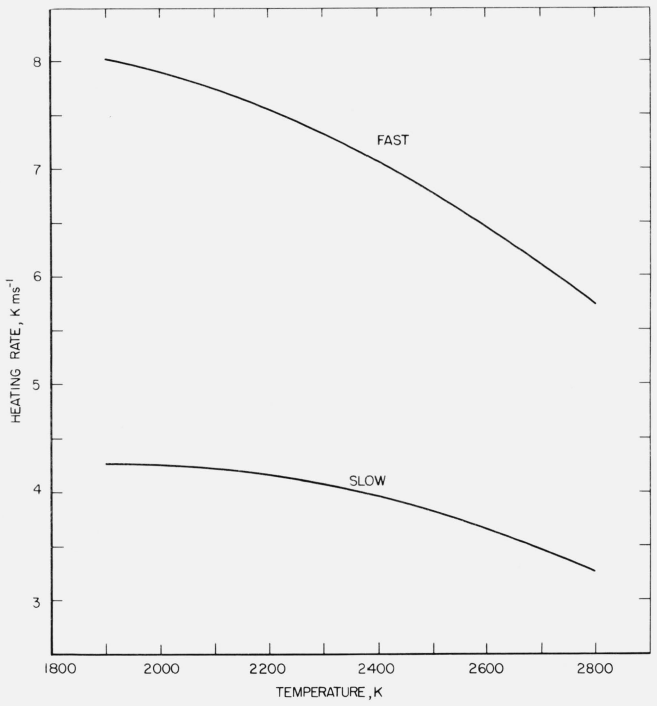

FIGURE 11. *Variation of the heating rate of a molybdenum specimen as a function of temperature.*

the entire measurement system. Reproducibility of the pulses was also determined by performing a total of 12 experiments at 5 min intervals. The maximum difference in the measured current values was less than 0.02 percent.

Although heating rate of the specimen depends, among other factors, on the power supply and the external circuit

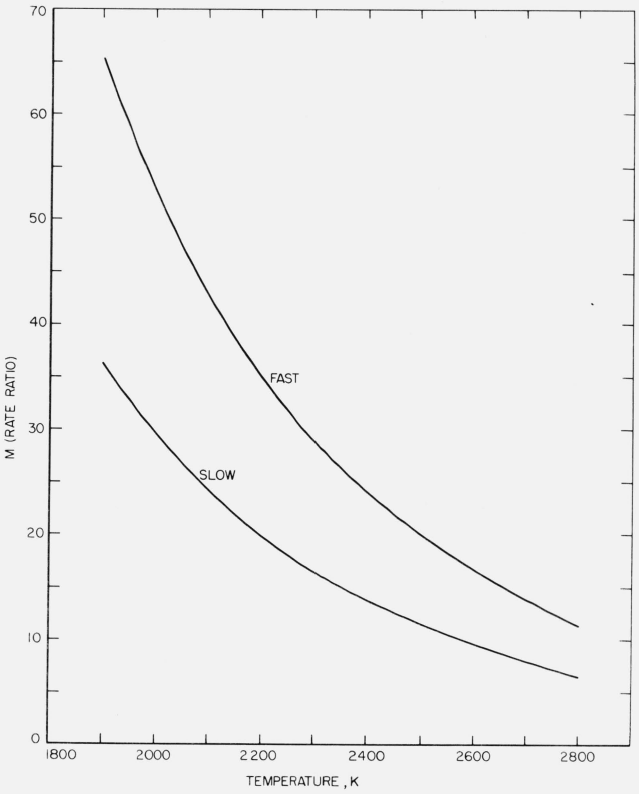

FIGURE 12. *Variation of the quantity M (ratio of heating to cooling rate) of a molybdenum specimen as a function of temperature.*

characteristics, the cooling rate following the opening of the switch depends on the specimen material and its geometry.

Power balance during cooling yields the following expression for the cooling rate of the specimen:

$$\left(\frac{dT}{dt}\right)_c = -BT^4 \tag{7}$$

where (8)

$B = \epsilon\sigma A/c_p n$
$A =$ effective surface area of specimen
$c_p =$ heat capacity
$n =$ weight of effective specimen
$T =$ specimen temperature
$\epsilon =$ hemispherical total emittance
$\sigma =$ Stephan Boltzmann constant (5.6697×10^{-8} W m^{-2} K^{-4})
$(dT/dt)_c =$ cooling rate.

The cooling rate as a function of temperature for a typical molybdenum specimen is shown in figure 13.

In order to obtain an expression for the specimen temperature during cooling as a function of time, eq (7) is rearranged and integrated. The resultant relation is

$$T = \left(\frac{1}{3Bt + \frac{1}{T_m^3}}\right)^{1/3} \tag{9}$$

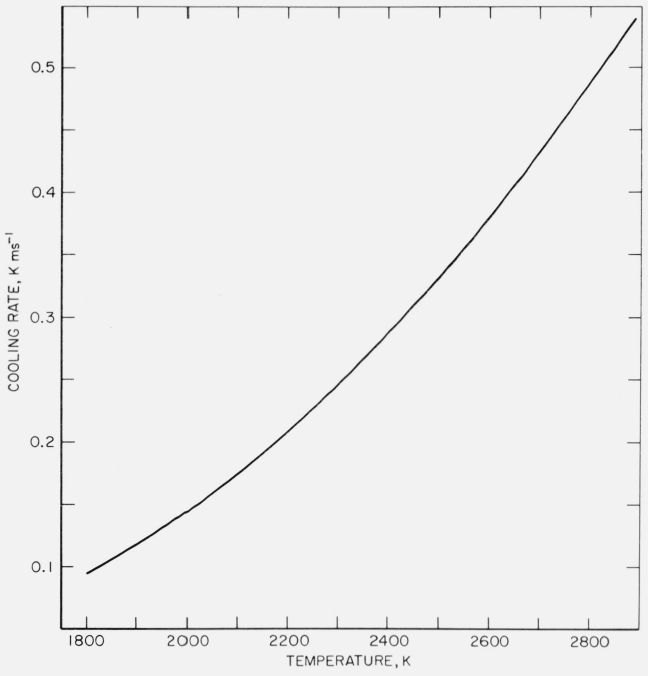

FIGURE 13. *Variation of the cooling rate of a molybdenum specimen as a function of temperature.*

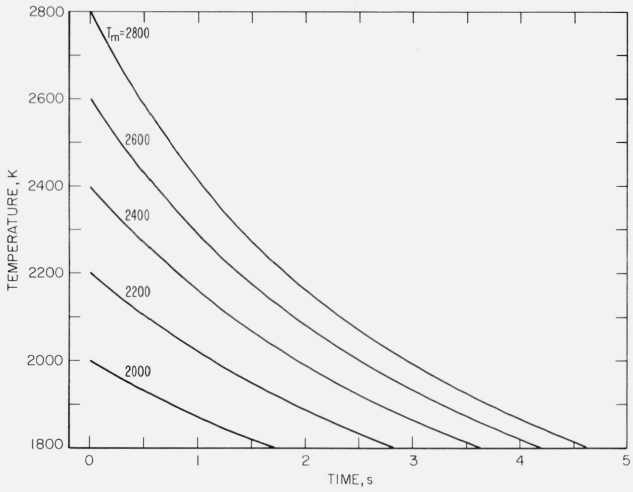

FIGURE 14. *Variation of the temperature of a molybdenum specimen during cooling from various initial temperatures.*

where

t = time

T_m = specimen temperature at the start of cooling (at $t = 0$).

Variation of the temperature of a molybdenum specimen during cooling as a function of time corresponding to different initial temperatures is shown in figure 14.

In preliminary calculations and also in computations related to error analysis it is necessary to know the quantity P_r/P_i, where P_r is power loss from the specimen due to thermal radiation and P_i is power input to the specimen. From power balances for heating and cooling periods the following relation is obtained:

$$\frac{P_r}{P_i} = \frac{1}{1+M} \tag{10}$$

where

$$M = \frac{(dT/dt)_h}{(dT/dt)_c}. \tag{11}$$

It may be seen that for the steady-state case $(dT/dt)_h = 0$, which implies that $M = 0$, and thus $P_r = P_i$.

4. Consideration of Various Phenomena

In this section various physical and electrical phenomena that affect the design and operation of high-speed thermodynamic measurement systems are presented.

4.1. Axial Temperature Distribution

Heat transfer from specimen to clamps causes the establishment of temperature gradients in the specimen. However, since the voltage probes are 12.7 mm away from the clamps, sharp temperature gradients near the clamps do not affect the measurements. The magnitude of the axial temperature gradient in the "effective" specimen is estimated by solving the transient heat conduction equation assuming constant properties and zero radial heat transfer [4]. The series solution is given by the following equation:

$$T = \left(\frac{i^2\rho l^2}{2\lambda A^2}\right)\left[1 - \frac{x^2}{l^2} - \frac{32}{\pi^3}\sum_{n=0}^{\infty}\frac{(-1)^n}{(2n+1)^3}\cos\left[\frac{(2n+1)\pi x}{2l}\right]\exp\left[-\frac{\alpha(2n+1)^2\pi^2 t}{4l^2}\right]\right] \tag{12}$$

where

i = electric current

ρ = electrical resistivity

A = cross-sectional area of specimen

l = half length of "effective" specimen

x = axial distance from midpoint of specimen

λ = thermal conductivity

α = thermal diffusivity.

If radial heat transfer is considered, the actual axial temperature gradient will be somewhat smaller than that given by eq (12).

The temperature gradient between the midpoint of the molybdenum specimen and various points along the specimen is calculated using eq (12) (with $n = 30$) for various heating pulses. The normalized results are shown in figure 15. Computations for heating pulses of 350 and 700 ms in duration indicate that specimen temperature at the plane of the potential probes is approximately 99.9 and 99 percent of its midpoint value, respectively. The respective average temperature of the "effective" specimen is 99.99 and 99.9 percent of its midpoint value.

To ascertain the temperature uniformity, a photograph of a molybdenum specimen was taken during the last part of the heating period. This photograph is shown in figure 16 in conjunction with the schematic of the specimen. No variations in exposure are detected for the portion between the potential probes. The region of sharp temperature gradients was studied photomicrographically. A photomicrograph of a molybdenum specimen, obtained after heating it to 2800 K for several times with pulses ranging from 0.4 to 0.8 s is shown in figure 17. Pertinent locations on the photomicrograph are identified with respect to the specimen. Two distinctly different grain structures may be seen. The portions of the specimen that were in the clamp or close to it have retained the original "drawn" pattern, while the portion that was heated to high temperatures shows a considerable grain growth. It is interesting to note a clear boundary between the two patterns, which correspond to a plane (P1) approximately 3 mm from the plane (P2) of the end clamp.

4.2. Radial Temperature Distribution

There is no exact solution for the time-dependent radial temperature distribution in conductors carrying pulse currents with radiative heat transfer from their surfaces. Even the numerical methods become very complicated because of the nonlinearity of the differential equation.

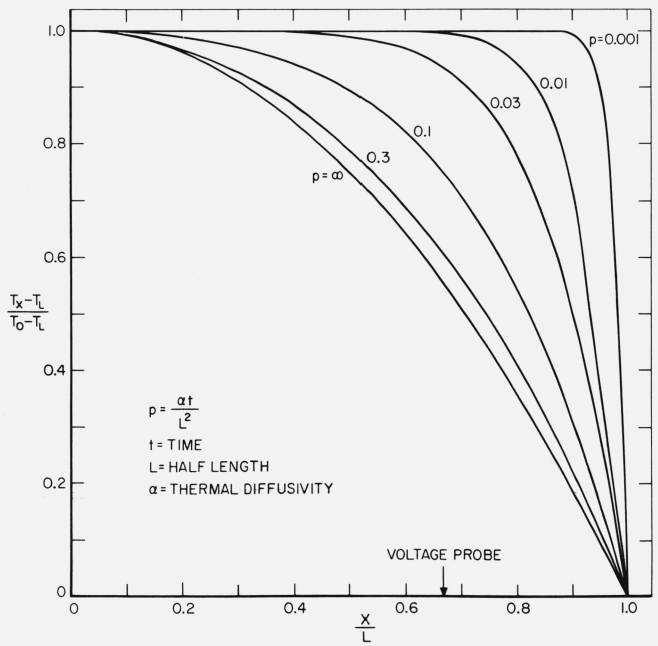

FIGURE 15. *Axial temperature distribution in a resistively self-heated specimen under transient conditions.*

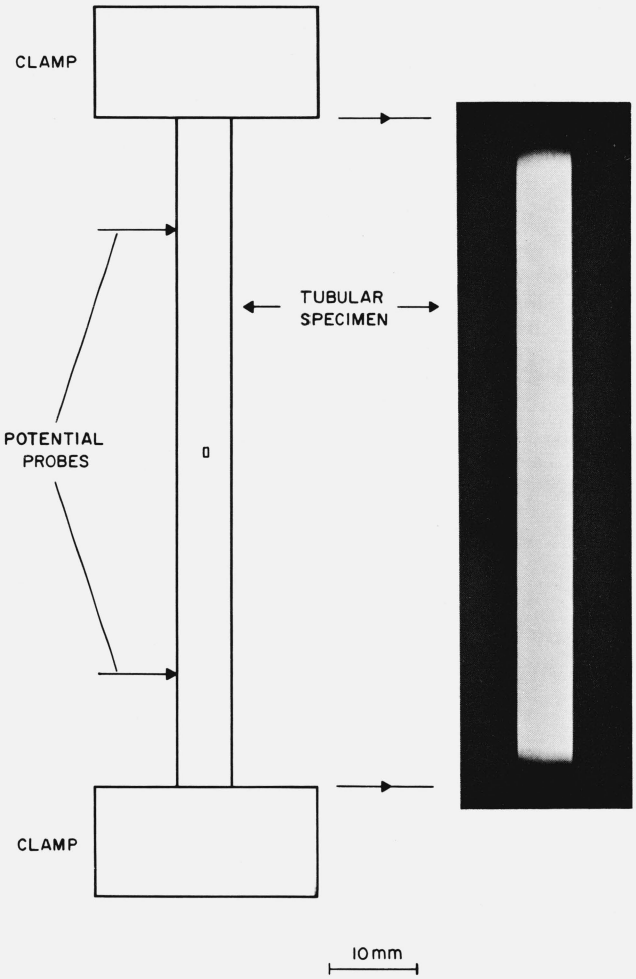

FIGURE 16. *Photograph of a molybdenum specimen during pulse heating to 2500 K.*

In pulse experiments where heat loss from the surface is small compared to power imparted to the specimen, the radial temperature drop (temperature difference between inner and outer surfaces for tubular conductors) may be estimated using the following approximate relation:

$$\Delta T_t = N\,\Delta T_s \qquad (13)$$

where

ΔT_t = temperature drop under transient conditions
ΔT_s = temperature drop under steady-state conditions
N = ratio of heat loss from the surface to imparted power under pulse conditions.

The solution of the steady-state radial heat conduction equation, assuming constant properties, for radial temperature drop is:

$$\Delta T_s = \frac{r_o \epsilon \sigma T^4}{2\lambda(r_o^2 - r_i^2)}\left[(R_o^2 - r_i^2) - 2r_i^2 \ln\left(\frac{r_o}{r_i}\right)\right] \qquad (14)$$

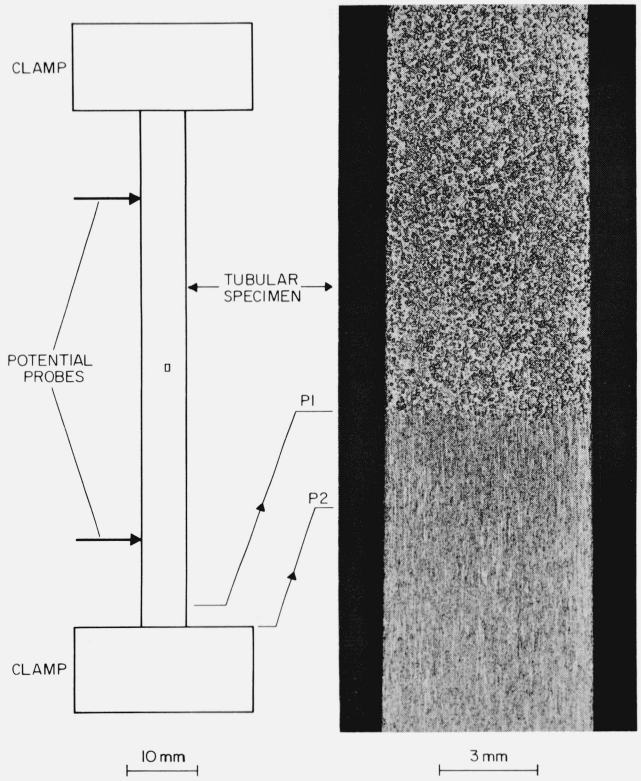

FIGURE 17. *Photomicrograph of a molybdenum specimen after pulse heating to 2800 K for several times.*

where

r_o = outer radius
r_i = inner radius
σ = Stephan-Boltzmann constant
ϵ = hemispherical total emittance
λ = thermal conductivity.

Computations on a molybdenum specimen indicate that radial temperature drop at 2800 K may be approximately 0.3 K for a heating pulse of 0.4 s.

4.3 Evaporation

The rate of evaporation $m(T)$ from metallic surfaces may be expressed by

$$m(T) = A\, e^{-E/T} \tag{15}$$

where, T is temperature in K, A is a constant for a given surface, and E is equal to the energy of evaporation in the units of the Boltzmann constant.

Since in high-speed experiments the heating period is short compared to the cooling period, one may assume that most of the evaporation takes place during cooling of the specimen. Total evaporation during cooling becomes

$$M = \int_{t_1}^{t_2} m(T)\, dt = \int_{t_1}^{t_2} A\, e^{-E/T} dt. \tag{16}$$

After performing a time-to-temperature transformation using eq (9) and integrating eq (16), one obtains

$$M = \frac{A}{BE^3}\left[e^{-\theta_m}\ (2 + 2\theta_m + \theta^2{}_m) - e^{-\theta_f}\ (2 + 2\theta_f + \theta^2{}_f)\right] \tag{17}$$

where

$$\theta_m = \frac{E}{T_m}$$

$$\theta_f = \frac{E}{T_f}$$

B = quantity expressed by eq (8)

and T_m and T_f are initial and final temperatures, respectively.

Computations on a molybdenum specimen indicate that the total weight loss due to evaporation during cooling from 2800 K is approximately 0.003 percent of the specimen weight.

4.4. Inductive Effects

Using equations given in the literature [5], self-inductance of the standard resistance and the specimen were computed to be 0.13 and 0.018 μH, respectively.

The maximum rate of change of the electric current during measurements in a typical high-speed experiment is approximately 3000 A s^{-1}. Then, the possible error (due to self-inductance) in potential measurements across the standard resistance and the specimen is 0.4 mV and 0.054 mV, respectively. Both of these values are smaller than the resolution of the recording system (1 mV).

In order to check the magnitude of mutual-induction between the main circuit and the signal circuits, the following experiment was performed. Potential connections to the standard resistance and the specimen were disconnected and were shorted duplicating, as much as possible, the geometrical configuration that the leads have during an actual high-speed experiment. A heavy pulse current was allowed to flow through the main circuit and the signals were recorded. The output of the recording system did not show any indication of voltage signals (within 1 mV resolution) that could have been generated as the result of mutual inductive coupling between the main circuit and the signal circuits.

4.5. Skin Effect

The skin effect, which is caused by changing currents in a circuit, alters the temperature distribution in the specimen.

For cylindrical conductors the skin effect is a function of the following parameter:

$$x = 2\pi a\sqrt{(2\mu f/10^9\rho)} \tag{18}$$

where

a = radius of the conductor
f = frequency of current
ρ = electrical resistivity of the specimen
μ = permeability of the specimen.

For nonmagnetic materials, $\mu = 1$.

In the case of tubular (thin-wall) specimens, the skin effect is a function of the following parameter:

$$\beta = x\,\tau/a\sqrt{2} \tag{19}$$

where

x = quantity defined by eq (18)
a = outer radius of the specimen
τ = thickness of the specimen.

In general, the contribution of the skin effect in a specimen is expressed in terms of the ratio of its electrical resistance at the frequency in question to that under d-c conditions. Results on the resistance ratio in terms of the parameter x and β are given in tabular form in the literature [5]. Computations indicate that for the specimen geometry and the type of pulses used in the present measurement system, the contribution of the skin effect is less than 0.01 percent.

4.6. Magnetic Forces

Magnetic force (per unit length) on a tubular specimen resulting from current flowing through it is expressed as

$$F = \left(\frac{4i^2}{3b}\right)\left[\frac{1+2m}{(1+m)^2}\right] \tag{20}$$

where i = current, $m = a/b$, b = outside radius, a = inside radius. The corresponding magnetic pressure is given as

$$P_m = \left(\frac{2i^2}{3\pi b^2}\right)\left[\frac{1+2m}{(1+m)^2}\right]. \tag{21}$$

Excessive magnetic forces, which act towards the center of the specimen, tend to collapse it. The collapsing pressure for thin-wall tubes is

$$P_c = \left(\frac{2E}{1-\mu^2}\right)(1-m)^3 \tag{22}$$

where E = modulus of elasticity and μ = Poisson's ratio.

The maximum allowable current is obtained by equating eqs (21) and (22), which yields

$$i = \sqrt{\left(\frac{3\pi b^2 E}{1-\mu^2}\right)\left[\left(\frac{1-m}{1+2m}\right)(1-m^2)^2\right]}. \tag{23}$$

4.7. Thermionic Emission

The contribution of thermionic emission is manifested in the following two forms: (1) energy loss from the specimen as a result of energy carried away by emitted electrons, (2) establishment of undesirable current paths around the specimen.

Dependence of thermionic emission current on temperature is given by

$$I = AT^2 e^{-\frac{e\phi}{kT}} \tag{24}$$

where

A = thermionic emission constant
ϕ = thermionic work function
e = electronic charge
k = the Boltzmann constant.

Considering the values $A = 55 \times 10^4$ A $m^{-2}K^{-2}$ and $\phi = 4.15$ eV [6,7] for molybdenum, thermionic emission current is computed to be approximately 7×10^{-5} A mm^{-2} at 2000 K and 0.15 A mm^{-2} at 2800 K.

It may be noted that computed values are for the case where electrons are continuously removed from the surface, which requires a collector plate at positive potential. In the present system, the chamber wall is electrically neutral and the only electrical potential gradient that exists is that across the specimen, which is less than 10 V. Thus, in the present experiments thermionic emission is most probably space charge limited; its contribution therefore would be much less than above computed values.

4.8. Thermoelectric Effects

Thermoelectric effects play an important role in experiments where temperature gradients exist and where currents flow through interfaces of dissimilar conductors. The Peltier effect between the specimen and clamps and the Thomson effect in the specimen where sharp temperature gradients exist are appreciable. However, they do not affect the measurements in the present experiments since their contribution is negligible in the "effective" specimen. To further reduce the possible contribution of thermoelectric effects, the knife-edges used for potential measurements are made of the same material as that of the specimen. In the high-speed experiments, the record of potential readings at high temperatures after the opening of the main switch shows "zero" for the potential between the probes. This indicates that there are no measurable erroneous signals due to the interaction (in thermoelectric sense) of the probes with the specimen.

4.9. Thermodynamic Equilibrium

Whether a specimen is under thermodynamic equilibrium while measurements are taken during rapid heating and cooling periods may be determined by considering the relaxation times of various rate processes.

Total relaxation time that must be considered for thermodynamic equilibrium calculations may be expressed as

$$\frac{1}{\tau} = \sum_i \frac{1}{\tau_i} \tag{25}$$

where each τ_i represents a different mechanism of relaxation. The various relaxation mechanisms are the results of different scattering processes. The main three relaxation processes are due to electron-phonon, electron-imperfection, and phonon-phonon interactions.

In electrical conductors, electron-phonon interaction is the predominant one in determining the overall relaxation time. For estimative purposes, the relaxation time due to this may be expressed as

$$\tau_{ep} = \frac{\sigma m}{ne^2} \tag{26}$$

where e = electronic charge, m = electronic mass, n = number of electrons per unit volume, and σ = electrical conductivity.

Relaxation time due to electron-phonon interactions for metals at room temperature is of the order of 10^{-12}s. Since relaxation time is directly proportional to electrical conductivity, and since the latter decreases with increasing temperature, it takes a longer time to establish thermal equilibrium at high temperatures. The variation of electrical conductivity in metallic elements between room temperature and their melting points is within a factor of 100; therefore, it can be seen that thermal equilibrium in metals takes place in times of the order of 10^{-10}s.

Information concerning relaxation times for vacancy equilibrium is not readily obtainable; but since the mechanism is related to that of diffusion, the relaxation time is an exponential function of temperature. The magnitude of vacancy relaxation time as observed in quenching experiments at lower temperatures and extrapolated to higher temperatures may be of the order of a millisecond for refractory metals above 2000 K.

5. Experimental Checks

The following sections outline the procedures and the results of selected experiments, which were performed to assess the accuracy of measured quantities under various operational conditions.

5.1. Resistance Comparison

The objective was to determine the value of a test resistance by measuring the current flowing through it and the voltage drop across its terminals under transient conditions and comparing this measurement with its resistance under steady-state conditions as determined by the potentiometric method.

In order to eliminate any doubt of the possibility of the effect of induced voltages on electrical signals, separate experiments were conducted using two geometrically different test resistances. One of the resistances (0.001 Ω) was a flat manganian strip identical to that used for pulse current measurements. The other was an Inconel tube with a nominal resistance of 0.003 Ω. The results on both test resistances do not indicate any dependence attributable to geometry. In these experiments pulse currents in the range 800 to 2100 A were used. The results do not indicate any current dependence. The results on resistance comparison and standard deviation of the measurements are shown in figures 18 and 19, respectively. It may be seen that, in general, resistance measurements by pulse and steady-state techniques are in agreement within 0.03 percent.

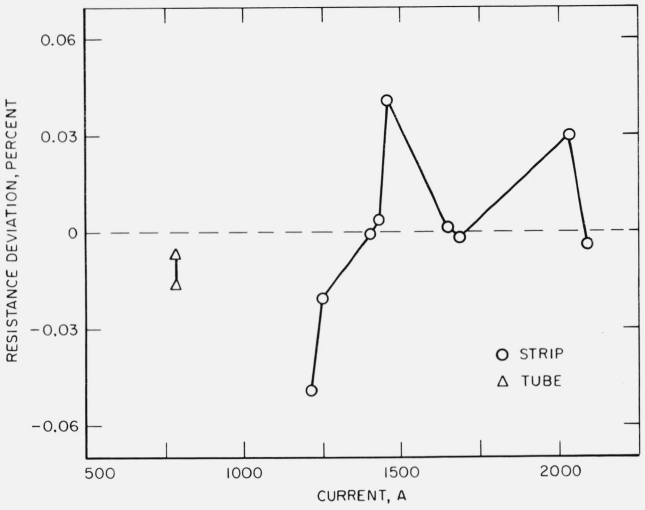

FIGURE 18. *Resistance difference of a test resistor measured under steady-state and pulse conditions.*

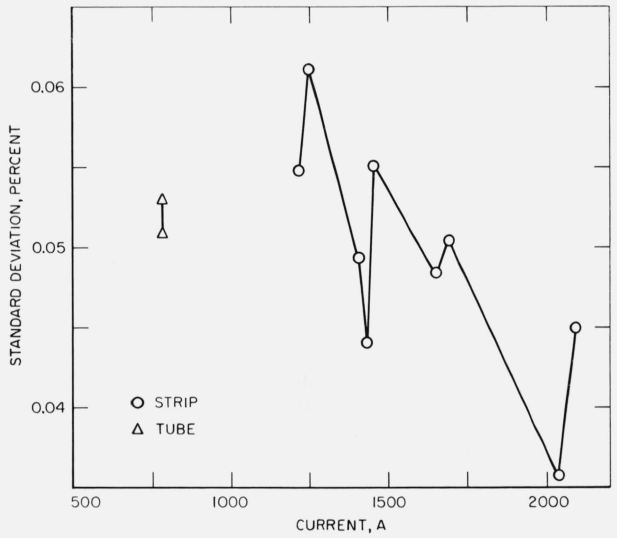

FIGURE 19. *Standard deviation of resistance measurements under pulse conditions.*

5.2. Effect of Different Heating Rates

Several phenomena depend upon the heating rate of the specimen. Heating rate is related, among other factors, to the electric current that flows through the specimen. In high-speed experiments, the rate of change of the current creates a number of problems such as induced voltages in measuring circuits, varying forces in the circuit components, etc. In addition to these extrinsic effects, there is the consideration of the specimen's attaining thermodynamic equilibrium at the time of measurements. To demonstrate partially that the above are negligible, in the present system under present operating conditions, the following experiments were conducted.

A tungsten strip (3.2 mm wide, 0.25 mm thick, 100 mm long) was placed in the high-speed measurement system. Two voltage probes were welded 20 mm apart at the center portion of the strip. Two pulse experiments were conducted in which the strip was heated from room temperature to 2200 K (surface brightness temperature) in approximately 2000 and 250 ms, respectively. During the experiments, quantities required for the determination of voltage, current, and surface brightness temperatures were recorded. Comparison of the resistances obtained from the two (slow and fast) experiments corresponding to the same brightness temperature yields the following average value:

$$R(\text{slow heating}) \,/\, R(\text{fast heating}) = 1.0003.$$

The resultant 0.03 percent deviation is within the uncertainty of resistance measurements. Thus, it may be concluded that approximately eightfold variation in the heating rate does not introduce any significant differences in the measured properties.

5.3. Melting Point of Platinum

As a partial check on the accuracy of temperature measurements, experiments were conducted to obtain the melting point of platinum. A high-purity (99.999 percent) platinum wire (diameter = 0.001 in, 0.025 mm) was wound (half turn) around a thin-wall molybdenum tube (similar to regular specimens) at the plane of the blackbody sighting hole. Two pulleys supported the wire. A 0.5 g weight was attached to each end of the wire to assure good contact between the wire and the tube. The ends of the platinum wire were connected to a special circuit, which indicated the time of the opening of the circuit resulting from the melting of platinum. The break in the circuit took place at a point of contact with the tube as the latter was pulse heated. Duration of an experiment (heating of the specimen from room temperature to its melting point) was approximately 0.8 s. Temperature of the tube corresponding to the time of the break in the platinum wire gave the melting point of platinum.

The results of three experiments gave an average value of 2044.2 K for the melting point of platinum on the 1968 International Practical Temperature Scale [8] with an average deviation from the mean of the three amounting to 1.1 K. This compares favorably with the accepted value of 2045 K [8]. Details regarding the experiments, interpretation of results, and errors are given in another publication [9].

6. Conclusions

Estimates indicate that the imprecision and inaccuracy of measured quantities in high-speed experiments using the present system are: 0.02 and 0.05 percent for voltage, 0.03 and 0.06 percent for current, and 0.5 K and 4 K for temperature at 2000 K.

The high-speed system described in this paper has been used successfully to measure heat capacity, electrical resistivity, hemispherical total and normal spectral emittances of molybdenum [1] and tantalum [11] from 1900 to near their respective melting points. The system was also used to obtain the melting point of molybdenum [12] and the variation of normal spectral emittance of tantalum during melting [13]. The results indicate that at 2000 K accuracy of measured properties by the system described here is about the same as that obtained by conventional methods. At temperatures above 2500 K, it surpasses any other method now known. Estimates of the imprecision and inaccuracy of measured properties are given in the above cited references.

7. References

[1] Cezairliyan, A., Morse, M. S., Berman, H. A., and Beckett, C. W., J. Res. Nat. Bur. Stand. (U.S.), **74A** (Phys. and Chem.), 65 (1970).
[2] Foley, G. M., Rev. Sci. Instr. **41,** 827 (1970).
[3] Morse, M. S., and Cezairliyan, A., in preparation.
[4] Carslaw, H. S., and Jaeger, J. C., Conduction of Heat in Solids (Oxford Univ. Press, Oxford, 1959).
[5] Grover, F. W., Inductance Calculations (Van Nostrand, New York, 1946).
[6] DuBridge, L. A., and Roehr, W. W., Phys. Rev. **42,** 52 (1932).
[7] Stanley, J. K., Electrical and Magnetic Properties of Metals, (Metals Park, Ohio, 1963).
[8] International Practical Temperature Scale of 1968, Metrologia **5,** 35 (1969).
[9] Cezairliyan, A., J. Res. Nat. Bur. Stand. (U.S.), **74C** (Eng. & Instr.), 87 (1970).
[10] De Vos, J. C., Physica **20,** 669 (1954).
[11] Cezairliyan, A., McClure, J. L., and Beckett, C. W., J. Res. Nat. Bur. Stand. (U.S.), **75A** (Phys. and Chem.), 1 (1971).
[12] Cezairliyan, A., Morse, M. S., and Beckett, C. W., Rev. Int. Htes. Tempér., to be published.
[13] Cezairliyan, A., High Temp.–High Pres., to be published.

(Paper 75C1-308)